Chapter 3

Synchrotron radiation

The purpose of this chapter is to introduce the phenomenon of synchrotron radiation, and its place in studies of radio-loud AGN. The derivations presented in Section 3.2 are not original – they owe much of their form to Longair (1994) – while those presented in later sections are the author's own developments starting from the work in Section 3.2.

First, a note: the derivations that follow are aimed at calculating the luminosity of synchrotron emission. This should (unless stated otherwise) be taken to mean the spectral luminosity, or luminosity per unit frequency, with SI units of W Hz^{-1}.

3.1 Introduction

In the 1940s, the development of experimental particle physics led to the development of various types of particle accelerators, which were used to accelerate particles such as electrons to high enough energies to observe particular interactions. One such form of accelerator that was common was the *synchrotron*, which used circular magnets to accelerate particles up to high energies – an early example was the General Electric 70 MeV synchrotron.

When these synchrotrons were first constructed and utilised, it was noticed (Elder et al. 1947, 1948) that an intense light (polarised in the plane of the electrons' orbit) was emitted from the high energy electrons. The theory of this radiation was investigated by Schwinger (1949), who first derived the spectrum of radiation that is emitted.

It was a few years later that its application to astrophysics was realised. Shklovsky (1953) showed that the radio and at least part of the optical emission of the Crab Nebula could be explained by synchrotron emission. It soon became accepted as the dominant component of the radio emission from the Galaxy, from supernova remnants, and from radio galaxies. The natural polarisation of synchrotron emission was used in a number of instances to confirm its presence, particularly at optical wavelengths (for example, Baade (1956) observed the polarisation of the jet in M87). A good review of the early studies of synchrotron emission is that by Ginzburg and Syrovatskii (1965), who, in this and their later review (Ginzburg and Syrovatskii 1969), tried to coin the term "magnetobremsstrahlung" as an alternative to "synchrotron". However, they did note that *"it hardly seems possible at this late stage to change the accepted terminology"*, and sadly, they proved to be correct.

3.2 Tangled magnetic fields

3.2.1 Introduction

The first derivation presented will be the derivation most commonly used in the literature. The method followed is that detailed in Longair (1994), which has the advantage of being done in S.I. units (unlike other derivations such as those found in Pacholczyk (1970) or Rybicki and Lightman (1979)).

The physical model for this derivation is a jet that has a tangled magnetic field. This means that there is no preferred angle to the magnetic field lines, and so we integrate over all viewing angles. The viewing angle is important because the radiation from each particle is strongly beamed in the direction in which that particle is travelling, since the particle is relativistic.

This relativistic motion means that the dipole radiation pattern that is emitted in the rest frame of the particle is Lorentz-transformed into a strongly beamed pattern in the observer's, or lab, frame (see Fig. 3.1). The way this pattern transforms is governed by the aberration formulae:

$$\sin\phi = \frac{\sin\phi'}{\gamma(1+\beta\cos\phi')}, \quad \cos\phi = \frac{\cos\phi'+\beta}{1+\beta\cos\phi'} \tag{3.1}$$

where a prime ($'$) indicates the particle's rest frame. In the rest frame, there is zero power emitted at angle $\phi' = \pi/2$, and so in the lab frame we have

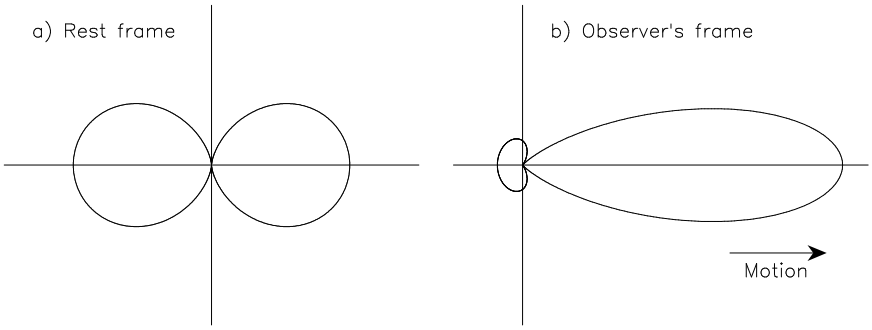

Figure 3.1: Diagram showing the effect of relativistic motion at right angles to acceleration. a) Dipole radiation pattern from a non-relativistic accelerated charge (i.e. in the particle's rest frame). b) Beamed radiation pattern from particle observed to be moving to the right. In this case, the particle is moving at a velocity of $0.4c$ (i.e. a Lorentz factor of just $\gamma = 1.091$), and the scale in both the x and y directions has been shrunk by a factor of two.

$\sin\phi = 1/\gamma$, which, for large γ (i.e. for a more relativistic particle), gives $\phi \sim 1/\gamma$. Thus all the forward power is radiated in a beam of angle $2/\gamma$. The emitted power as a function of angle is also affected by the relativistic motion of the particle. The full expression is not shown here, but it results in very strong power emitted in the forward direction, and much less power in the opposite direction (see Fig. 3.1).

3.2.2 Derivation

We first consider the case of a single particle (of mass m, energy $E = \gamma mc^2$, and charge e) moving with velocity v in a uniform magnetic field of strength B. The trajectory of this particle makes an angle of α_p with the direction of the magnetic field – this angle is called the "pitch angle". The particle's trajectory forms a spiral, or helix, centred on the field line, due to the $\vec{v} \times \vec{B}$ force. This spiral has a radius of curvature, with respect to the central line, of $a = v/(\omega_r \sin\alpha_p)$, where $\omega_r = eB/m\gamma$ is the relativistic gyro-frequency.

The emission can be expressed in terms of components in two polarisations: both perpendicular and parallel to the projected direction of the magnetic field. A rather complete derivation of these two components is given in Longair (1994) – here we simply give the final result. Defining two variables to be used in the equations:

$$\theta_\gamma^2 = 1 + \gamma^2\theta^2 \qquad \eta = \omega a \theta_\gamma^3 / 3c\gamma^3,$$

we can write these two emission components as:

$$\frac{\mathrm{d}I_{\perp}(\omega)}{\mathrm{d}\Omega} = \frac{e^2\omega^2}{12\pi^3\epsilon_0 c}\left(\frac{a\theta_\gamma^2}{c\gamma^2}\right)^2 {K_{\frac{2}{3}}}^2(\eta) \tag{3.2}$$

$$\frac{\mathrm{d}I_{\parallel}(\omega)}{\mathrm{d}\Omega} = \frac{e^2\omega^2\theta^2}{12\pi^3\epsilon_0 c}\left(\frac{a\theta_\gamma}{c\gamma}\right)^2 {K_{\frac{1}{3}}}^2(\eta) \tag{3.3}$$

where $K_{\frac{1}{3}}$and $K_{\frac{2}{3}}$are the modified Bessel functions of order $\frac{1}{3}$ and $\frac{2}{3}$ respectively.

The next step is to integrate over solid angle. Since nearly all the radiation is emitted within very small angles of the pitch angle (due to the relativistic beaming of the radiation pattern), and the elemental solid angle varies little over $\mathrm{d}\theta$, the solid angle becomes $\mathrm{d}\Omega = 2\pi\sin\alpha_p\mathrm{d}\theta$. We can then integrate Eqns. 3.2 & 3.3 with respect to θ. Also, since the radiation is concentrated in a small angle about α_p, we can take the integral limits to $\pm\infty$ (as this makes finding an analytic solution that much easier!). Thus:

$$I_{\perp}(\omega) = \frac{e^2\omega^2a^2\sin\alpha_p}{6\pi^2\epsilon_0 c^3\gamma^4}\int_{-\infty}^{+\infty}\theta_\gamma^4 {K_{\frac{2}{3}}}^2(\eta)\mathrm{d}\theta \tag{3.4}$$

$$I_{\parallel}(\omega) = \frac{e^2\omega^2a^2\sin\alpha_p}{6\pi^2\epsilon_0 c^3\gamma^2}\int_{-\infty}^{+\infty}\theta^2\theta_\gamma^2 {K_{\frac{1}{3}}}^2(\eta)\mathrm{d}\theta \tag{3.5}$$

[Note that by integrating over solid angle, we are evaluating the total power radiated by the particle, in all directions, which, while useful for the case of a tangled field, is not necessarily what is desired when calculating observed synchrotron spectra from a uniform field. This point will be addressed in Section 3.3.]

By using analytic integrals (Westfold 1959), these two quantities can be written in terms of the functions

$$F(x) = x\int_x^{\infty} K_{\frac{5}{3}}(z)\mathrm{d}z \qquad \text{and} \qquad G(x) = xK_{\frac{2}{3}}(x) \tag{3.6}$$

(where $x = 2\omega a/3c\gamma^3 = 2\eta/\theta_\gamma^3$). We therefore obtain

$$I_{\perp}(\omega) = \frac{\sqrt{3}e^2\gamma\sin\alpha_p}{8\pi\epsilon_0 c^3}(F(x)+G(x))$$

$$I_{\parallel}(\omega) = \frac{\sqrt{3}e^2\gamma\sin\alpha_p}{8\pi\epsilon_0 c^3}(F(x)-G(x))$$

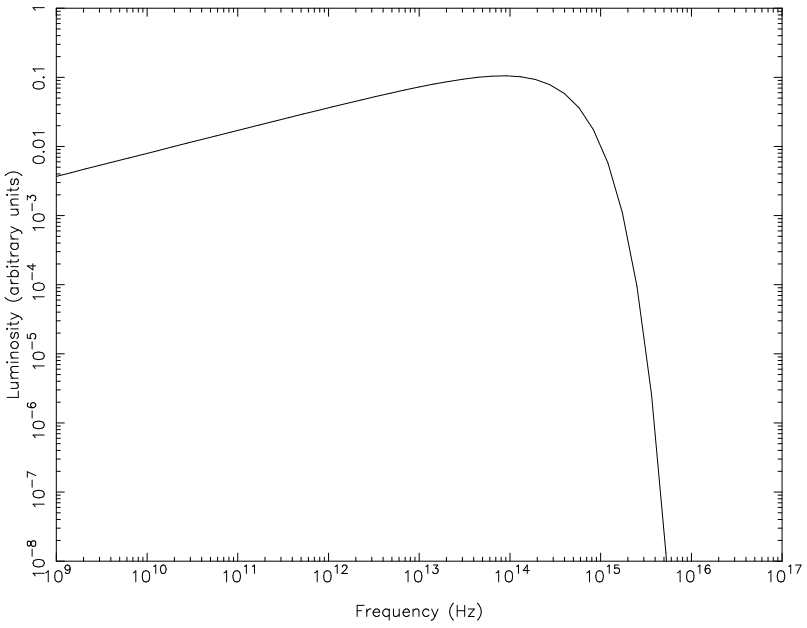

Figure 3.2: Synchrotron spectrum of a single particle in a tangled magnetic field. Values of the parameters are: $B = 10^{-4}$T, $\gamma = 10^4$, and $\alpha_p = 45°$.

The next and final step in deriving the single particle emission function is to add these terms and divide by the time over which the radiation was emitted. Since we have integrated over solid angle, the above expressions give the energy emitted during one period of the particle's orbit, i.e. in a time $T_r = \nu_r^{-1} = 2\pi\gamma m/eB$. Thus, the total luminosity (i.e. radiated power) of the particle in both polarisations is:

$$L(\omega) = \frac{I_\perp + I_\parallel}{T_r} = \frac{\sqrt{3}e^3 B \sin\alpha_p}{8\pi^2\epsilon_0 cm} F(x) \tag{3.7}$$

This flux is shown in Fig. 3.2, for $B = 10^{-4}$T, $\gamma = 10^4$, and $\alpha_p = 45°$.

3.2.3 Populations

This equation gives the emission spectrum for a single particle in a magnetic field. More interesting, from an astronomical point of view, is the spectrum from a *population* of particles. Such a population will have a distribution of energies (and hence Lorentz factors) and pitch angles. The two most commonly used distributions are a power law distribution of energies, $N(E)\mathrm{d}E = \kappa E^{-p}\mathrm{d}E$, and an isotropic probability distribution of pitch

angles, $p(\alpha_p) = \frac{1}{2}\sin\alpha_p$.

We can then integrate over energy and pitch angle to obtain the total emission from such a population. This is done in detail by Longair (1994), but we just quote here the result for the dependence of the resulting flux on both frequency and magnetic field strength:

$$L_{\rm pop}(\nu) \propto B^{(p+1)/2}\nu^{-(p-1)/2} \tag{3.8}$$

This is a very important result, as it links an observable parameter (i.e. the spectral index of the emission) to the power law slope of the particle energy distribution, in the sense that $\alpha = (p-1)/2$ (where we use α to represent the spectral index, as is standard in the literature). We will come back to this result in the next section.

Note that a power law distribution of energies produces a power law emission. In physical systems, however, the energy distribution can often either cut off, or change slope at some energy. A good example for this comes from the modelling done by Meisenheimer et al. (1996) on the radio to optical emission from the jet of M87. They found that the best fit to the flux measurements was for an energy distribution of the form $N(\gamma) \propto \gamma^{-2.31}$, with an abrupt cut off at some maximum energy.

In general, if the energy distribution has a cut off, then the resulting emission spectrum will have a critical frequency ν_c where the power law spectrum has an exponential cutoff (in the same manner as the single particle spectrum – see Fig. 3.2). It can be shown (for example, Blandford 1990) that this critical frequency scales like $\nu_c \propto \gamma_+^2 B$, where γ_+ here is the maximum value of the γ distribution.

3.3 Ordered jets

The derivation in Section 3.2 integrates over all the possible viewing angles. This is valid if the magnetic field in which the particles are moving is tangled (i.e. there is no preferred direction of the magnetic field), or if you are interested in the total energy radiated from a region. In the former case, there will be particles moving in many different directions, and so the observer will see contributions from many different values of the viewing angle θ.

However, if the magnetic field is not tangled, but is instead quite uniform,

the observer will only see emission in a small range of θ values, those close to the angle between the line of sight and the magnetic field direction. Such a physical set-up may be similar to that seen in the collimated jets of FR II radio galaxies, or in the high-polarisation regions of both radio and optical jets. To find the observed spectrum for this case, we need to take into account only that radiation which is beamed in the direction of the observer.

The total energy emitted as a function of viewing angle is given by the sum of Eqns. 3.2 & 3.3. To obtain the observed luminosity (that is, the emitted power per unit frequency) of a single particle, we divide this by the orbital time $T_r = \nu_r^{-1} = 2\pi\gamma m/eB$. We use this time since the observer will see a pulse of emission (corresponding to the beamed radiation pattern) once in every orbit of the helical path of the emitting particle. This gives the following:

$$\begin{aligned} L_{1p}(\omega,\theta,\gamma) &= \frac{eB}{2\pi\gamma m}\frac{e^2\omega^2}{12\pi^3\epsilon_0 c}\left(\frac{a\theta_\gamma}{c\gamma}\right)^2\left[\frac{\theta_\gamma^2}{\gamma^2}{K_{\frac{2}{3}}}^2(\eta)+\theta^2{K_{\frac{1}{3}}}^2(\eta)\right] \\ &= \frac{e^3B\omega^2}{24\pi^4\epsilon_0 cm\gamma}\left(\frac{m\beta\gamma}{eB\sin\alpha_p}\right)^2\frac{\theta_\gamma^4}{\gamma^4}\left[{K_{\frac{2}{3}}}^2(\eta)+\frac{\theta^2\gamma^2}{\theta_\gamma^2}{K_{\frac{1}{3}}}^2(\eta)\right] \\ &= \frac{e\ m\ \omega^2}{24\pi^4\epsilon_0 Bc\sin^2\alpha_p}\frac{\beta^2\theta_\gamma^4}{\gamma^3}\left[{K_{\frac{2}{3}}}^2(\eta)+\frac{(\theta_\gamma^2-1)}{\theta_\gamma^2}{K_{\frac{1}{3}}}^2(\eta)\right] \end{aligned}$$

So, if for simplicity we let $\zeta = em/(24\pi^4\epsilon_0 c)$, then the power per unit frequency for a single particle, as a function of frequency ($\nu = \omega/2\pi$), angle ($\theta = \phi - \alpha_p$, where ϕ is the line-of-sight angle to the magnetic field direction) and energy ($E = \gamma mc^2$) is given by:

$$L_{1p}(\omega,\theta,\gamma) = \frac{\zeta\,\omega^2}{B\sin^2\alpha_p}\frac{\beta^2\theta_\gamma^4}{\gamma^3}\left[{K_{\frac{2}{3}}}^2(\eta)+\frac{(\theta_\gamma^2-1)}{\theta_\gamma^2}{K_{\frac{1}{3}}}^2(\eta)\right]. \qquad (3.9)$$

3.3.1 Populations

Once again, we want to look at the emission from a population of particles, rather than just a single particle. We use the distributions of energy and pitch angle used for the previous case.

Energy

The energies of the particles in the population are assumed to be distributed according to a power law (here we write it in terms of γ, rather than E). In this case, however, the power law is assumed to cut off at some maximum energy γ_+:

$$N(\gamma)\ \mathrm{d}\gamma = \begin{cases} \kappa\gamma^{-p}\ \mathrm{d}\gamma & 1 \leq \gamma \leq \gamma_+, \\ 0 & \gamma > \gamma_+. \end{cases} \tag{3.10}$$

Pitch Angle

The pitch angles are assumed to have an isotropic distribution. This is given by the probability distribution

$$p(\alpha_p)\ \mathrm{d}\alpha_p = \frac{1}{2}\sin\alpha_p\ \mathrm{d}\alpha_p$$

In general, the distribution of pitch angles will be defined by (or at least related to) the process by which the particles are accelerated.

Due to the beaming of the emission, an observer is only going to see emission from particles with pitch angles very close to $\alpha_p = \phi$. That is, the range of α_p values is restricted to a small range $\alpha_{p_1} - \alpha_{p_2}$, where $\alpha_{p_1} = \phi - \delta\alpha_p$ and $\alpha_{p_2} = \phi + \delta\alpha_p$. In practice, since these integrals are calculated computationally, we can determine the value of $\delta\alpha_p$ empirically by finding where the flux drops below some cutoff level. We find that $\delta\alpha_p$ is roughly proportional to the inverse square-root of the frequency (at higher frequencies, the emission becomes slightly more beamed, and so the width of the integration does not need to be as great), so that

$$\delta\alpha_p = 10^{-3}\left(\frac{\nu}{(10^{10}\mathrm{Hz})}\right)^{-\frac{1}{2}}, \tag{3.11}$$

where $\delta\alpha_p$ is measured in radians.

Total emission

To obtain the total emission from such a population, we integrate over both the energy and the pitch angle, to find:

$$L_{\rm tot}(\omega,\phi) = \int_{\alpha_{p_1}}^{\alpha_{p_2}} \frac{1}{2}\sin\alpha_p \left(\int_1^{\gamma_+} \kappa\gamma^{-p} L_{1p}(\omega,\gamma,\phi-\alpha_p)\ \mathrm{d}\gamma\right)\ \mathrm{d}\alpha_p$$
$$= \frac{\zeta\,\omega^2\kappa}{2B}\int_{\alpha_{p_1}}^{\alpha_{p_2}}\int_1^{\gamma_+} \frac{\beta^2\theta_\gamma^4\gamma^{-p-3}}{\sin\alpha_p}\left[{K_{\frac{2}{3}}}^2(\eta) + \frac{(\theta_\gamma^2-1)}{\theta_\gamma^2}{K_{\frac{1}{3}}}^2(\eta)\right]\mathrm{d}\gamma\,\mathrm{d}\alpha_p, \tag{3.12}$$

where $\theta = \phi - \alpha_p$. See the following section for example spectra.

3.4 Exploring parameter space

Examination of Eqn. 3.12 shows that the luminosity at frequency ω of a population of particles depends on a number of factors: the viewing angle ϕ (that is, the angle the line of sight makes with the direction of the magnetic field); the particle energy distribution (governed in this case by the parameters p and γ_+); and the magnetic field strength B in the region of emission. In this section, we will examine each of these individually, to try to determine the dependence the luminosity has on each of them.

3.4.1 Variation of viewing angle

The viewing angle, or angle of the $\vec{B}$ vectors to the line of sight, is an important physical quantity, since jets are long, thin structures and will be inclined at some angle to the line of sight. See Section 2.2.2 for some typical values for jets that have been observed at optical wavelengths. Note that in measuring the viewing angle with respect to the direction of the jet, we are assuming that the magnetic field lies along the jet (i.e. parallel to the jet's direction). While this is obviously going to be a simplification of real jets, observations of M87 (Perlman et al. 1999) indicate that the magnetic field does tend to be parallel to the jet direction, particularly in the inter-knot regions.

In Fig. 3.3, we see the variation of the spectrum with changing viewing angle ϕ. Shown are spectra in units of both L_ν (luminosity per unit frequency) and L_λ (luminosity per unit wavelength), in arbitrary luminosity

units.

Because the L_λ spectra rise to a peak and then decrease (this peak is related to the critical frequency ν_c mentioned earlier), we can use the location of the peak to find dependencies on ϕ of both the normalisation of the flux, and the location of the peak wavelength. We find that both these quantities depend on $\sin\phi$ in the following manner:

$$\lambda_{\rm peak} \propto (\sin\phi)^{-1} \tag{3.13}$$

$$L_{\lambda,{\rm peak}} \propto (\sin\phi)^{2.5} \tag{3.14}$$

Also, the shape of the spectrum is independent of the viewing angle, so that the entire curve has the same flux–angle dependence.

3.4.2 Variation of magnetic field strength

Another important physical quantity is the magnetic field strength B. A strong magnetic field will increase the strength of the synchrotron emission, as well as affect the location of the turnover. Magnetic fields in jets are often estimated assuming "equipartition", where the energy densities of the electrons and the magnetic field are equal. Typical values obtained are $\sim 10^{-4}{\rm G} = 10^{-8}{\rm T}$, although it is thought that values less than this are required to account for observed synchrotron cooling (e.g. in the M87 jet Heinz and Begelman (1997)). The value of the magnetic field is likely to increase as you move in towards the compact core.

In Fig. 3.4, we see the variation in the spectra as the magnetic field strength varies from 10^{-4}T to 10^{-11}T. The peak wavelength varies with B as

$$\lambda_p \propto B^{-1} \tag{3.15}$$

The peak flux, however, does not show a simple power law variation with B, but rather shows some curvature over the range of values explored. At large values of B ($B > 10^{-7}$T), the flux goes like $L_p \propto B^{2.5}$, while at lower values ($B < 10^{-8}$T), the relationship is $L_p \propto B^3$.

3.4.3 Variation of energy distribution

The energy distribution (Eqn. 3.10), being a power law up to a maximum energy, has two parameters: γ_+, the maximum energy, and p, the slope of

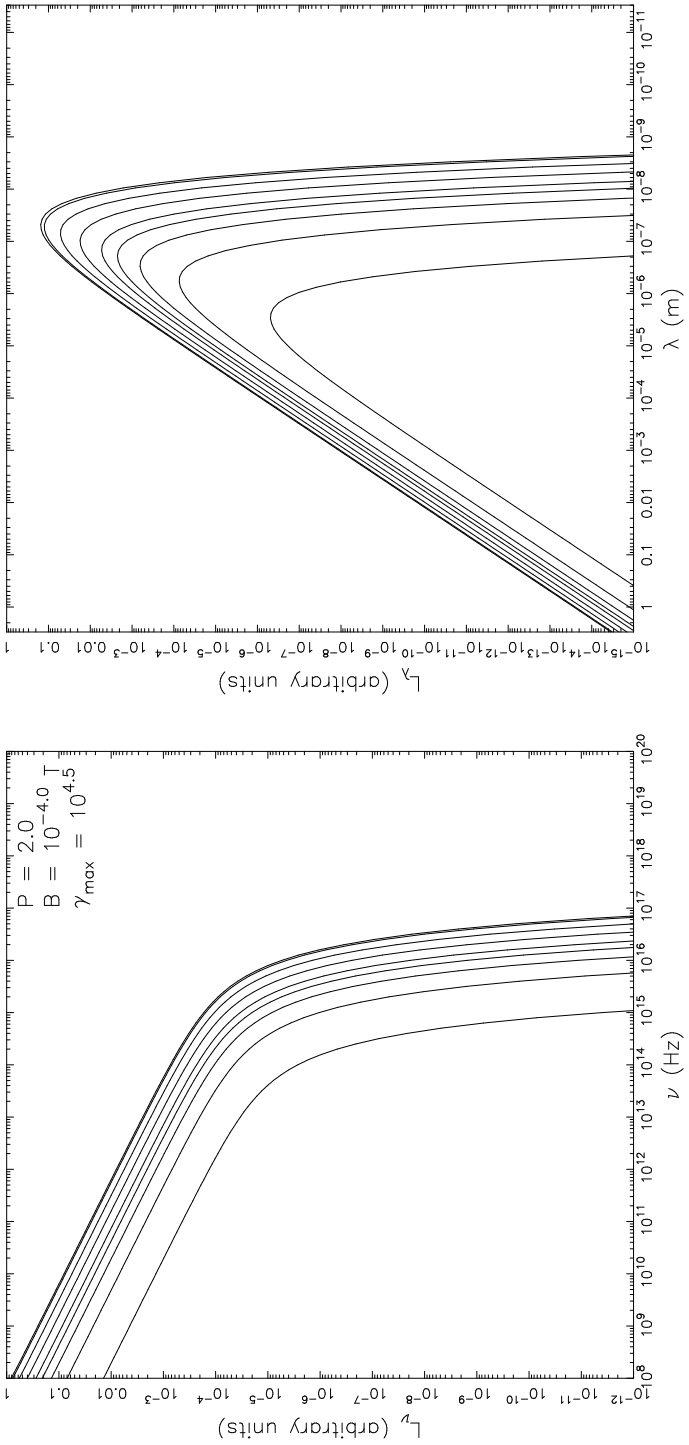

Figure 3.3: Variation of luminosity with changing viewing angle ϕ, which takes the values 90°, 70°, 45°, 30°, 20°, 15°, 10°, 5° and 1° (with larger ϕ values giving larger fluxes). The values of the other key parameters are indicated.

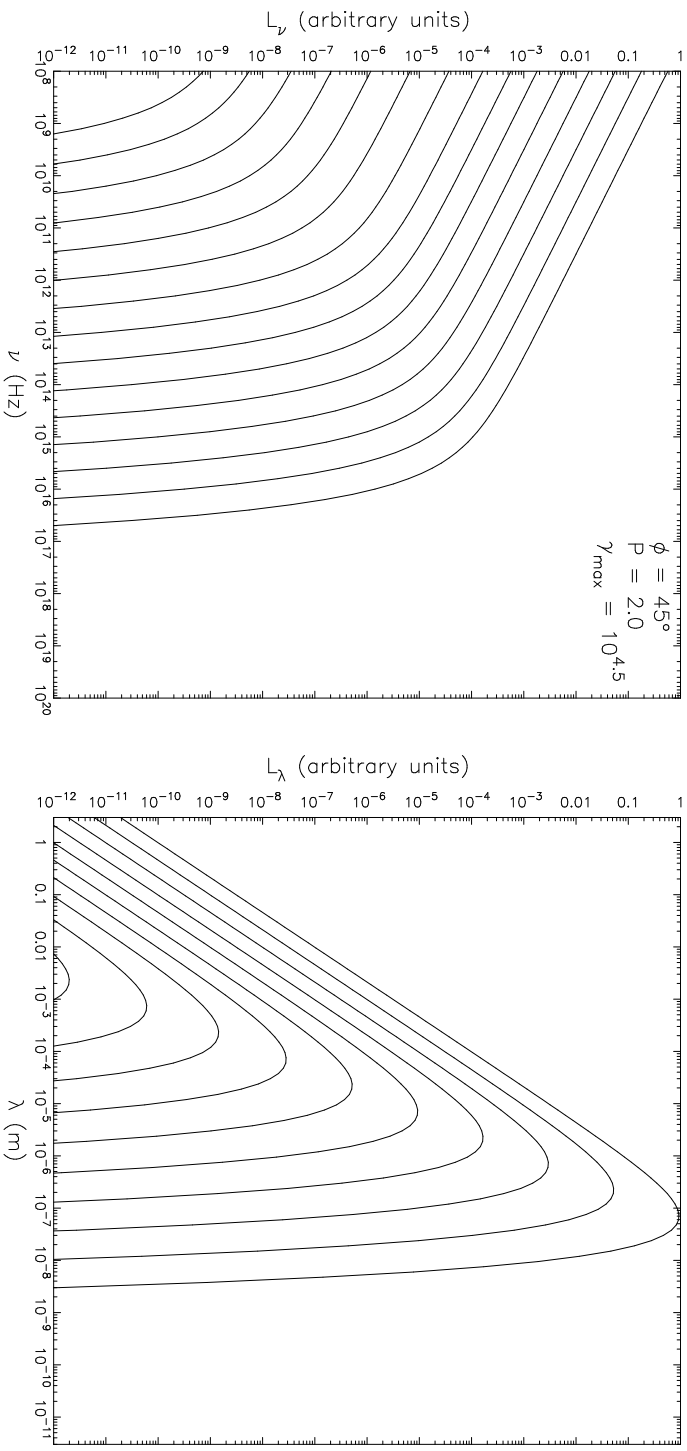

Figure 3.4: Variation of synchrotron spectrum with changing magnetic field strength B. The values of B considered are every half-dex in the range 10^{-4}T to 10^{-11}T, with higher B values giving higher fluxes. The values of the other key parameters are indicated.

the power law. We need to investigate what dependence the spectrum has on both of these parameters.

Maximum energy

The maximum energy of the energy distribution will strongly affect the resulting synchrotron emission, as the higher energies will contribute at the high-frequency end. A lack of high energy particles, therefore, will result in a spectrum that turns over at lower frequencies.

A range of synchrotron spectra with different γ_+ values are shown in Fig. 3.5. Note that, for wavelengths longer than the peak, the power law slope is the same, but the different γ_+ values cause the spectrum to turn over at different points. Once again, we can look at how the peak wavelength and flux vary with γ_+, and we find (looking at the L_λ spectra):

$$L_{\lambda,\mathrm{peak}} \propto \gamma_+^3 \tag{3.16}$$

$$\lambda_{\mathrm{peak}} \propto \gamma_+^{-2} \tag{3.17}$$

Slope of power law

The slope of the power law determines how rapidly the energy spectrum drops off with increasing energy. A large value of p means a steeper power law slope, which means that the higher energies are less prominent in the particle population. The value of p will affect the slope of the synchrotron spectrum at frequencies $\nu \ll \nu_c$.

The spectra for different values of p are shown in Fig. 3.6, from $p = 1$ (the one with the largest luminosity) up to $p = 4.5$ (the least luminosity). As can be seen, the synchrotron power law index α gradually steepens as p increases, and we find that the relationship between the two indices is $\alpha = (p-1)/2$, which is the same as that for the tangled field case (Section 3.2).

Also worth noting is the fact that the location of the peak does not change with the different values of p. This removes one degree of freedom in choosing the location of the peak/turnover frequency of the synchrotron emission.

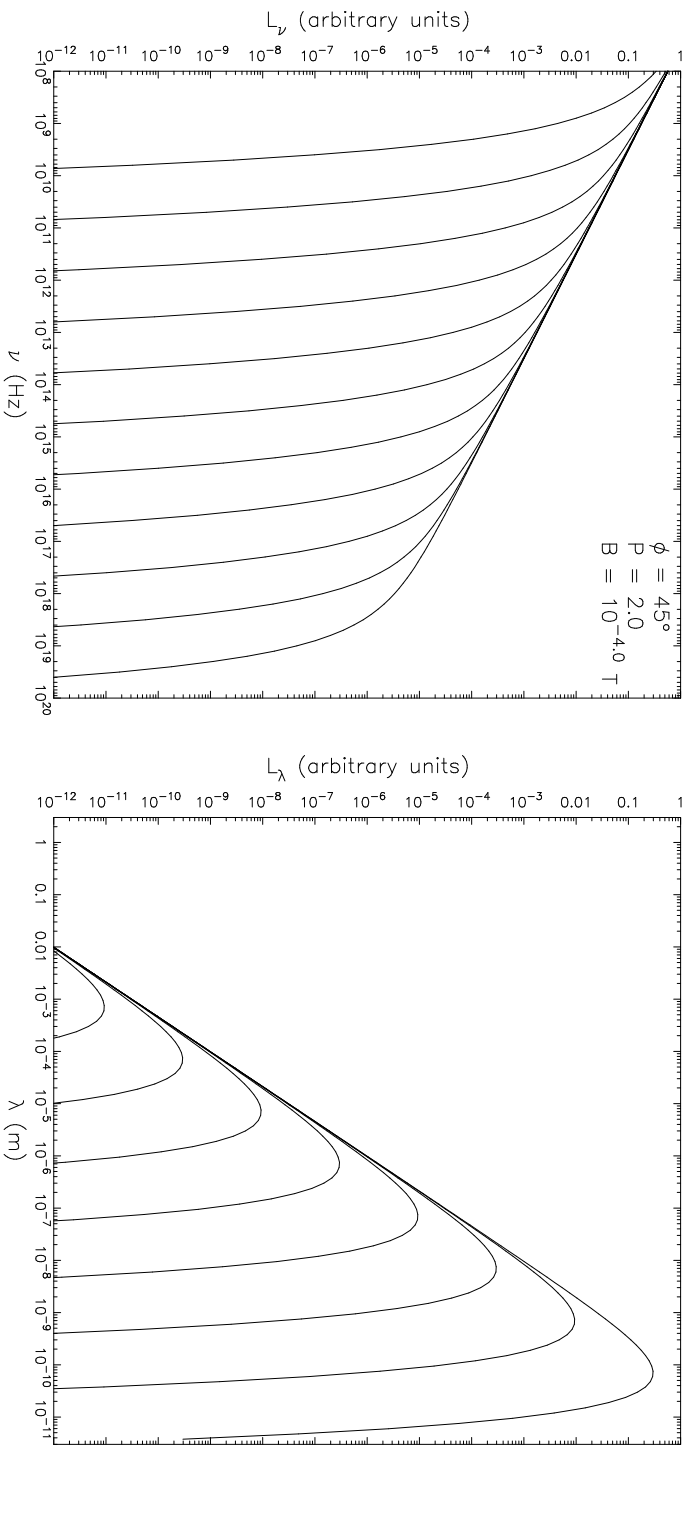

Figure 3.5: Variation of synchrotron spectrum with changing maximum energy γ_+. The values of γ_+ considered are every half-dex in the range 10 to 10^6, with the higher γ_+ values giving spectra extending to higher frequencies. The values of the other key parameters are also indicated.

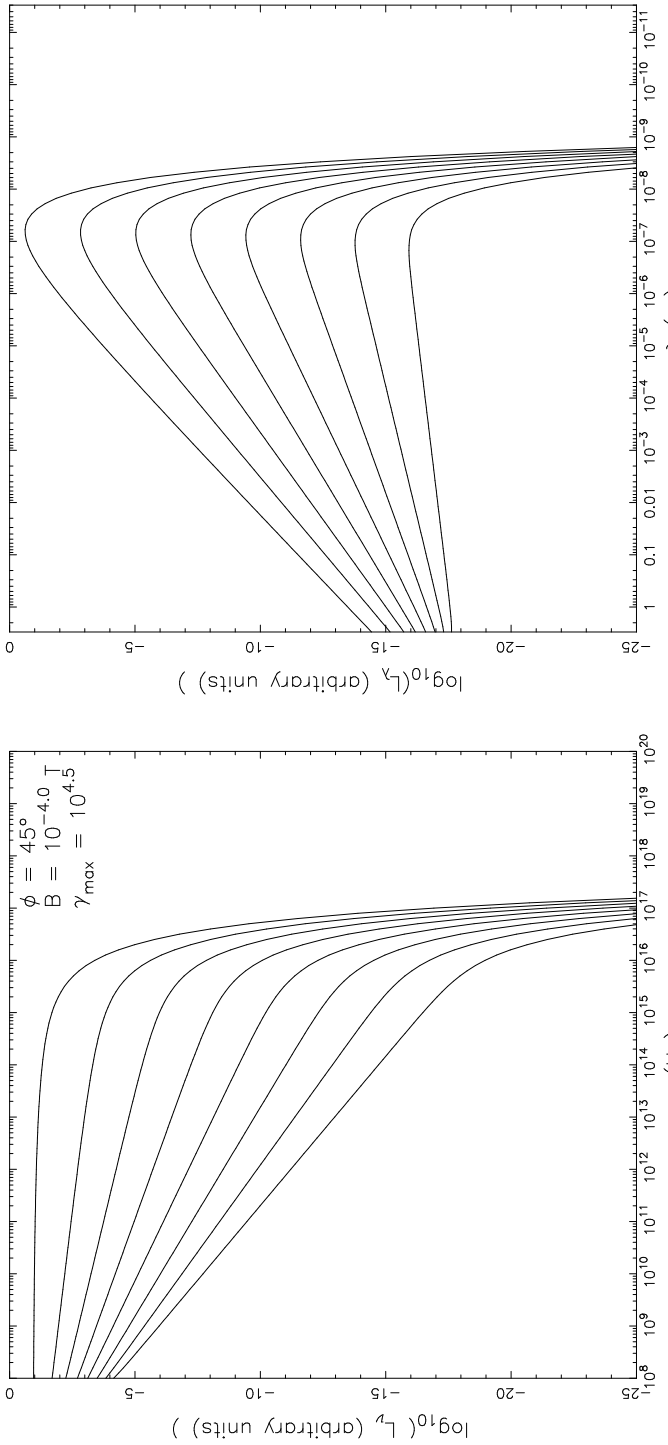

Figure 3.6: Variation of synchrotron spectrum with changing p. The values of p are spaced every 0.5 in the range 1 to 4.5, and the larger the value of p, the steeper and lower in flux is the resulting spectrum. The values of the other key parameters are also indicated. Note that this graph has a vertical axis that is different from the other graphs.

3.4.4 Overall variation

If we combine all these variations together, we can find how the peak wavelength and the peak flux vary with all the physical parameters. The net dependency is:

$$\lambda_{\text{peak}} \propto \gamma_+^{-2} B^{-1} \sin\phi^{-1} \tag{3.18}$$

or, in terms of frequency:

$$\nu_c \propto \gamma_+^2 B \sin\phi$$

This has the same dependency as the tangled field derivation, although with the added dependence on the line of sight angle. This angle is also crucial in determining the overall luminosity, due to the strong dependence found: $L \propto (\sin\phi)^{2.5}$. This is worth noting carefully, since for small angles to the line of sight the overall luminosity will decrease quite rapidly. This is the opposite effect that you get from Doppler boosting, an enhancement of intensity coming from a source moving relativistically towards the observer. This effect is discussed in the following section.

3.5 Relativistic Doppler boosting

The calculations up to now have been made in the rest frame of the jet, i.e. there is no bulk motion present. However, in real jets, relativistic bulk motion has been postulated to exist, mainly from observations of superluminal motion in radio jets. Various models have been developed (Lind and Blandford 1985; Urry and Padovani 1995) to explain how the observed emission from a jet with bulk motion is affected, and we investigate two of the standard models in this section.

For a relativistic source moving at an angle ϕ to the line of sight, with a Lorentz factor $\Gamma = 1/\sqrt{1-\beta^2}$ (where $\beta = v/c$), the observed flux is enhanced by the Doppler factor

$$\delta = \frac{1}{\Gamma(1 - \beta\cos\phi)} \tag{3.19}$$

The degree of enhancement depends on the nature of the source, but, in the case of a continuous, collimated jet (such as is modelled in Section 3.3), it takes the form

$$F_\nu(\nu) = \delta^{2+\alpha} F'_{\nu'}(\nu),$$

where a $'$ indicates a quantity is measured in the rest frame, $\nu = \delta\nu'$, and $F_\nu \propto \nu^{-\alpha}$. The other basic model for beaming is the case where, instead of a continuous jet, the outflow occurs in discrete "blobs". The beaming then has the form

$$F_\nu(\nu) = \delta^{3+\alpha} F'_{\nu'}(\nu).$$

Note that here, Γ is the *bulk* Lorentz factor, which relates to the velocity of features moving along the jet, not the velocities of the individual particles (which have Lorentz factors γ). This may be due to some bulk flow of plasma, or, in the latter case, the velocities of the individual "blobs".

Note that as $\phi \to 0$, the value of δ increases, reaching a maximum value at $\phi = 0$ of $\delta_{\max} = 1/\Gamma(1-\beta) \approx 2\Gamma$ for $\beta \approx 1$. The effect of Doppler boosting is shown in Fig. 3.7, for two extreme cases: $\delta^{2.5}$, corresponding to a continuous jet with $\alpha = 0.5$; and δ^4, corresponding to a jet made up of discrete blobs with $\alpha = 1.0$. The flux in these plots are normalised to the $\Gamma = 1$ curve, corresponding to isotropic emission. Note that for increasing Γ, the flux at small angles rapidly increases, whereas the large angle flux decreases below the un-boosted flux (the so-called "de-beaming"). The case of a larger dependence on δ (the discrete blob case) shows a much larger dependence on angle.

However, in the case of synchrotron emission from an ordered field, this dependence is counteracted by the angular dependence of the emission itself. To find the angular dependence of the observed flux, we need to take into account the fact that beaming changes the observed angle (in the manner of the aberration formulae Eqn. 3.1). The flux observed at an angle ϕ in the observer's frame will depend on both the Doppler beaming factor and the flux emitted at angle ϕ' in the rest frame of the blob/jet. These angles are related by (inverting Eqn. 3.1):

$$\begin{aligned}\sin\phi' &= \frac{\sin\phi}{\Gamma(1-\beta\cos\phi)} \\ &= \delta\sin\phi\end{aligned}$$

Thus, the observed flux at angle ϕ is

$$\begin{aligned}F(\phi) &\propto \delta^p(\sin\phi')^{2.5} \\ &\propto \delta^{p+2.5}(\sin\phi)^{2.5}\end{aligned}$$

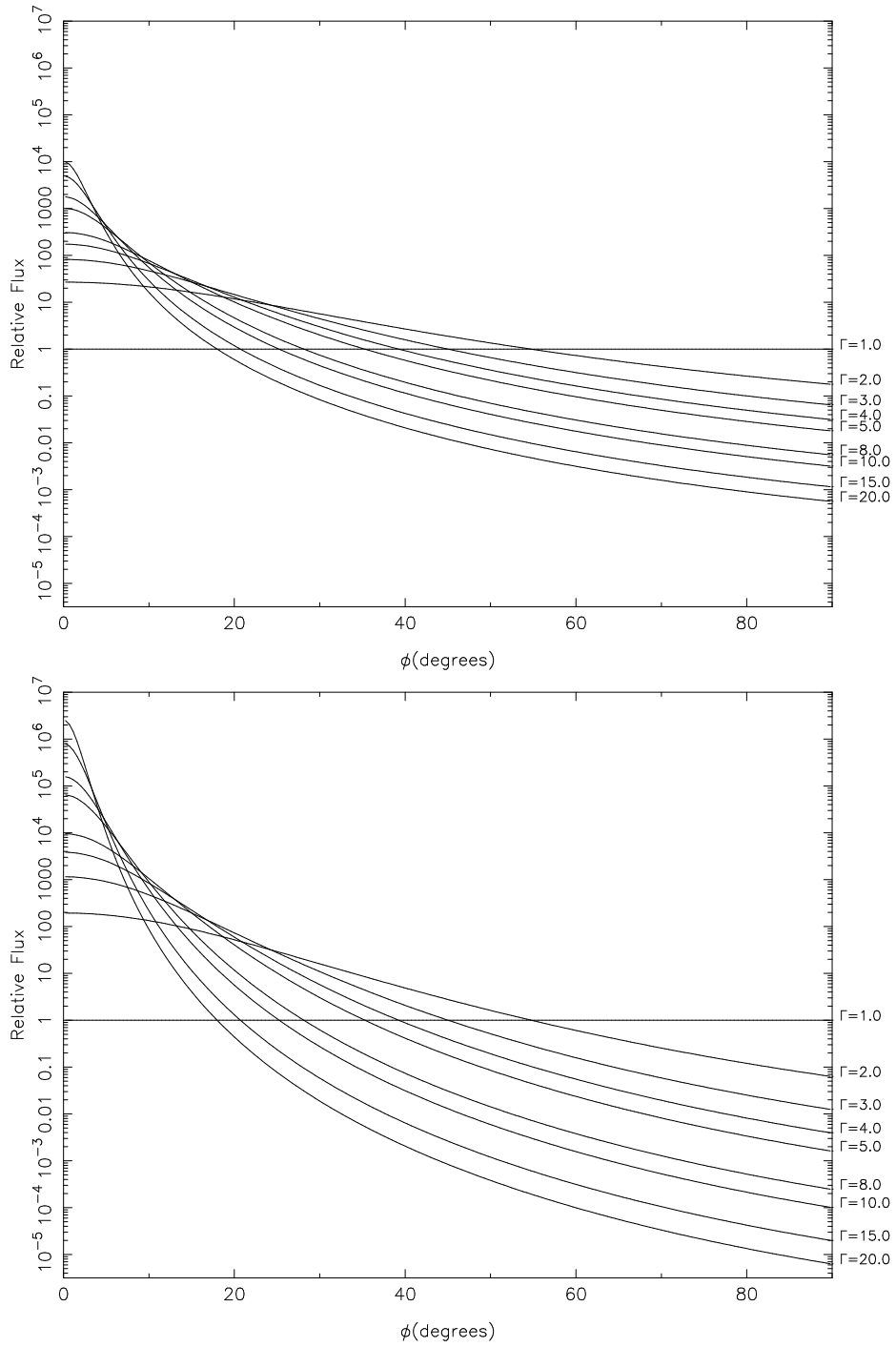

Figure 3.7: The effect of Doppler boosting on isotropic emission, for two different dependencies on δ: $\delta^{2.5}$ in the top plot and δ^4 in the bottom. The amount of Doppler boosting for each curve is shown by the value of the bulk Lorentz factor Γ next to the terminating point of the curve. A value of $\Gamma = 1$ represents no Doppler boosting.

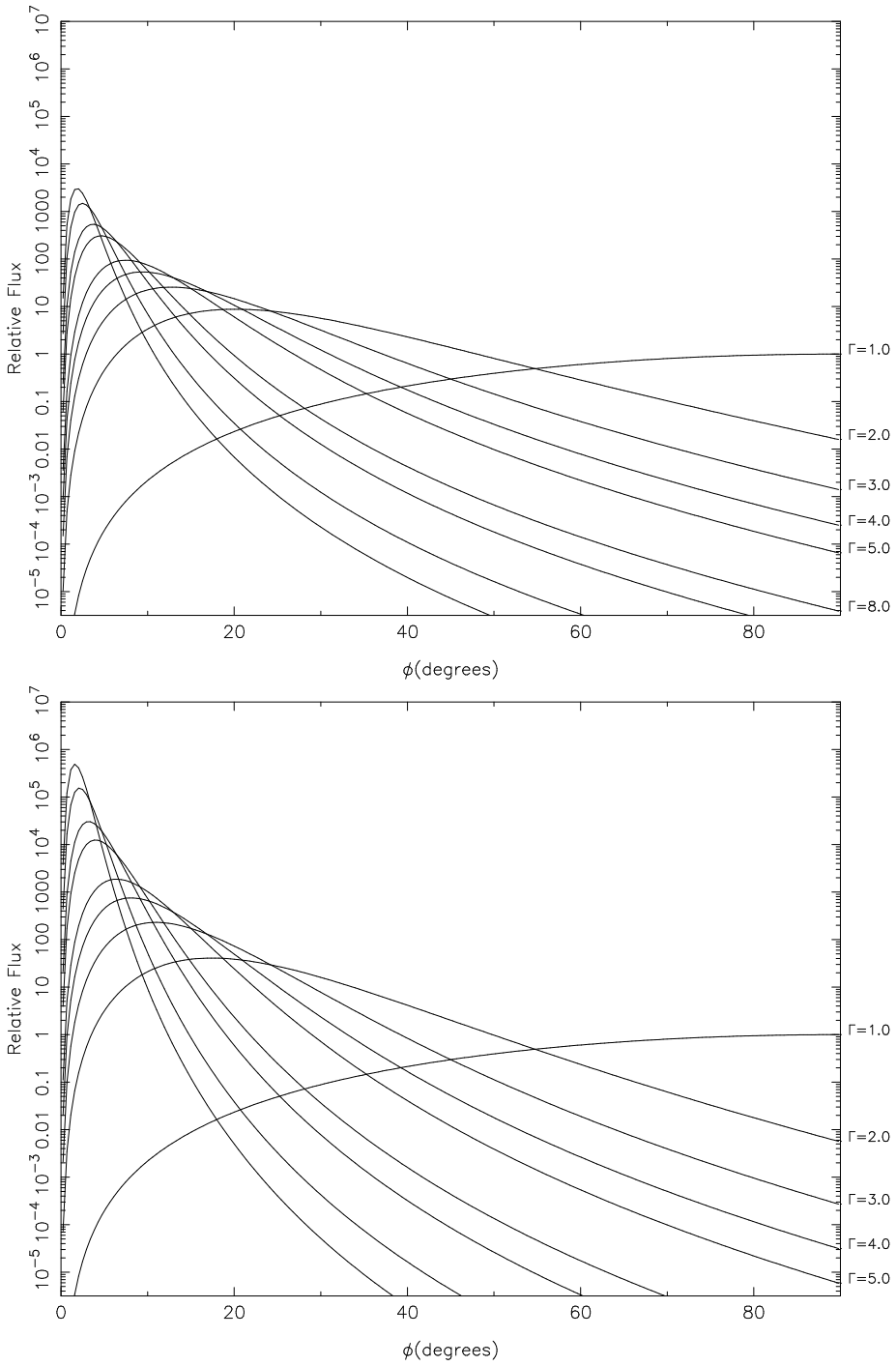

Figure 3.8: The effect of Doppler boosting combined with the angular dependence of the ordered field synchrotron emission (Section 3.3), for two different dependencies on δ: $\delta^{2.5}$ in the top plot and δ^4 in the bottom. The Γ values are the same as for Fig. 3.7. A value of $\Gamma = 1$ represents no Doppler boosting.

where p is either $2 + \alpha$ or $3 + \alpha$ depending on the nature of the source (see above).

Fig. 3.8 shows the angular dependence of the flux for various amounts of boosting, parametrised by the Lorentz factor Γ, for the same two cases of Fig. 3.7. The flux is normalised to the observed flux at an angle of 90°with no boosting (that is, with $\Gamma = 1$). As can be seen, when the angular dependence is considered by itself, the flux rapidly decreases for small ϕ. As more and more Doppler boosting is added, the flux at small angles increases, due to both the intensity enhancement and the angular aberration. The boosted flux approaches that of the isotropic emission case near the peak of the curve, but drops rapidly at low angles. Also noticeable is that the de-beaming effect is more pronounced for this case, so that most of the flux is observed in a small range of angles. As Γ increases, this angular range gets smaller, and moves to smaller ϕ values

3.6 Discussion

There are a number of key points to arise from this analysis. Firstly, consider the effect that the angular dependence of the synchrotron emission has on the observed flux. In the case of pure Doppler boosting (Fig. 3.7), the flux at small angles to the line of sight is boosted by factors of up to several orders of magnitude (depending on the bulk velocity, the spectral slope and the physical makeup of the jet). However, when this is combined with the angular dependence of synchrotron emission from an ordered magnetic field (Fig. 3.8), the observed flux at small angles decreases rapidly. The angles at which this occurs become smaller for larger values of the bulk velocity Γ. The flux at large angles is also reduced more, due to enhanced de-beaming.

Thus, for an ordered jet to be viewed at angles close to its direction of motion (assuming the magnetic field is parallel to that direction), a reasonably large bulk velocity (i.e. large Γ) is required. A jet with a low value of Γ will still have a significant decrease in flux at low values of ϕ due to the strong angular dependence of the emission.

Secondly, we note that jets, particularly those seen in double-lobed radio sources (i.e. such as those in FR IIs), are seen at large angles to the line of sight. At large angles, the Doppler beaming becomes, in effect, de-beaming, since the observed flux is reduced. This observation, then, puts a strong

restriction on how large the values of Γ can be in the jet. For large enough Γ, the de-beaming will be sufficient to reduce the jet flux to levels too small to be observed. Also, this effect applies for both types of synchrotron emission (both tangled and ordered fields – in fact it is more pronounced for the ordered field case), and for all types of beaming (i.e. different dependences on δ).

Finally, since much of the work presented in this chapter has been concerned with synchrotron emission from an ordered magnetic field, is there any observational evidence that such emission will be important in astrophysical contexts? There are two particular observations that point to there being magnetic fields that are quite highly ordered in the jets of AGN.

The first of these observations is the measurement of high values of polarisation in both the radio and optical – parts of the M87 jet have $P \sim 40\% - 50\%$. Such high polarisations imply that the magnetic field is highly ordered. Further examples are the high optical and NIR polarisations measured from quasars ($P \sim 20\%$ – see Chapter 6). These measurements are made by integrating over the entire source, and so imply the existence of regions of highly ordered magnetic fields.

The second observation is that some jets, particularly those in the powerful FR II radio galaxies, are highly collimated. Collimation of a jet can be caused by either pressure from the ambient medium, or magneto-hydrodynamic confinement. While the ambient medium is likely to be important for the weakly confined jets in FRI radio galaxies, it is unlikely that it can provide the necessary collimation seen in the thin jets in FR II sources. This collimation can most likely only be provided by highly structured magnetic fields that confine the jet to its thin, well collimated shape. Both this observation and that of high polarisation point to ordered magnetic fields being important in the jets of radio-loud AGN.